Postprint of: Czaja Z., A method of fault diagnosis of analog parts of electronic embedded systems with tolerances, Measurement, Vol. 42, Iss. 6 (2009), pp. 903-915, DOI: 10.1016/j.measurement.2009.01.014

A method of fault diagnosis of analog parts of electronic embedded systems with tolerances

Zbigniew CZAJA*

Gdansk University of Technology, Faculty of Electronics, Telecommunications and Informatics,
Department of Optoelectronics and Electronic Systems,
ul. G. Narutowicza 11/12, 80-952 Gdansk, Poland

Abstract

A new method of fault detection and localization of analog parts with tolerances of non-faulty elements in embedded mixed-signal systems controlled by microcontrollers is presented. The method consists of three stages. In the pre-testing stage a fault dictionary is created. The measurement stage bases on the measurements of duration times of output signals of analog comparators realized by internal resources of the microcontroller. The time response to a stimulating square impulse of the analog part is applied to the inputs of the comparators with different threshold voltages. In the last stage the fault detection and localization is performed by the microcontroller. The main advantage and novelty of the method is the fact that the BIST consists only of analog comparators and internal resources of the microcontroller already mounted in the system. Hence, this approach simplifies the structure and design of BISTs, which allows to decrease test costs. The results of experimental verification of the method are included in the paper.

Keywords: fault diagnosis, built-in self-test (BIST), microcontrollers

1. INTRODUCTION

At present, electronic embedded systems are applied in almost all spheres of human life. Actually, they already have dominated markets**:** automotive, aviation, multimedia, telecommunication, medical, etc. So, fault tests and fault diagnoses are fundamentally important for these systems.

* Corresponding author. Tel.: +48-58-347-14-87; fax: +48-58-347-22-55.
E-mail address: zbczaja@pg.gda.pl

The testing procedures of the electronic embedded system regard to functional testing of the whole system [1], the software testing [2,3] and testing of particular blocks of the system [4]. One of these blocks is an analog part which is used mostly to adjust input analog signals usually coming from sensors and passed on to analog-to-digital conversion blocks.

A fault diagnosis of analog parts bases on fault diagnosis methods of analog circuits with limited computational possibility of the embedded system. So, simulation-before-test methods are often used. For analog circuits, the lack of simple fault models, the presence of component tolerances and circuit nonlinearities are major problems which make the elaboration of testing or self-testing methods of analog parts difficult. For embedded systems, where often there is no direct access to the analog part (to its internal nodes), measurements of proprieties of the analog part can be realized only by additional blocks called Built-In Self-Testers (BISTs). Testing or self-testing of analog parts based on BISTs is very difficult and not standardized. It follows from the variety of analog circuits and their applications. In addition, the offered BISTs are dedicated, only for selected not numerous classes of circuits, particularly for analog to digital converters (ADCs) where usually BISTs have a more complex structure than the ADCs [5-8] and also for digital to analog converters (DACs) [9], where the built-in BIST structure enables calibration and fault detection. For analog filters and amplifiers generally three types of BISTs are used:

- Based on sigma-delta modulators [10,11], where the BISTs consist of ΣΔ modulators, low-pass analog filters, ADCs, DACs and digital blocks.
- Based on the oscillation-test methodology [12-17]. In this case the analog circuit is transformed into an oscillator by adding a feedback path and modifying the circuit either adding or removing some passive components. Additionally a digital circuit, which measures deviations of the frequency of oscillation of the tested circuit, should be built into the BIST.
- Based on test strategy using power spectral analysis [18]. The tested circuit is stimulated by a noise generator, its response is sampled by an ADC and the estimation of the power spectrum density based on the fast Fourier transform is realized by a DSP microprocessor.

The feature of BISTs mentioned above is hardware excess and great requirements relating to computing power. It causes increased production costs of the systems. Hence, in the paper a new fault diagnosis method is proposed for analog circuits for which the BIST is realized by already existing resources of embedded electronic systems. Such approach allows to minimize the test cost and guarantees a high quality of products.

The presented idea bases on the fact that usually control units in the form of microcontrollers are used to control simple embedded systems. So, it is profitable to use their hardware resources to create the BIST and their computing power to realize testing or self-testing procedures of the analog part.

2. PRINCIPLE OF THE METHOD

As mentioned above, the microcontrollers serve controlling and processing functions in many applications of electronic embedded mixed-signal systems.

Thus, we can use hardware resources (peripheral devices) and the computing power of such a microcontroller to realize the measurement microsystem testing the analog part assembled on a printed circuit board [19].Therefore, we obtain a flexible and reconfigurable BIST, which is created only during the testing time. Beyond this time, the microcontroller with its internal devices perform normal functions appointed by the program controlling the embedded system. Hence, we significantly decrease the number of elements of the BIST which should be added to the system to create a typical BIST [10-18].

It is possible thanks to the use of a new class of methods of fault detection and localization of single soft faults of passive elements in analog linear circuits, where [19]:

- The stimulating square impulse is generated by the control unit. Its duration time T is determined by the internal timer of this control unit.
- Measurements of the duration time τ_k of the output signal of each k–th analog comparator (with the threshold voltage v_k) are performed by the internal timer of the control unit, where k=1,..,K and K is the number of all analog comparators connected to the output of the analog part (see Fig. 1).
- Each k–th output signal is a conversion result of the k–th analog comparator of the time response of the analog part to the square impulse.
- Fault detection and localization procedures are realized also by the control unit based on the measurement result, the fault dictionary and the diagnosis procedure located in its program memory.

In this approach the digital signal is treated as an analog stimulus and the analog response of the tested circuit is converted to the digital domain by a set of K analog comparators (Fig. 1). So, in this case the BIST requires only the addition of analog comparators to the system.

The author elaborated also an approach which uses the internal analog-to-digital converter (ADC) of the microcontroller [20] instead of external analog comparators. In this case the tested analog part is also stimulated by the square impulse generated by the microcontroller, but the response signal is directly sampled K times by the ADC precisely at the moment established by its internal timer. So, we obtain the measurement result treated as the measurement point with coordinates (u_1, u_2, .., u_K). In the diagnosis procedure this point with the fault dictionary are used for fault detection and localization.

Thus, in both approaches we have the same way of stimulation of the tested analog circuit, but different ways of extraction of information about the tested circuit. The measurement time and computing

complexity for both methods is the same, as also the size of the fault dictionary (for the same K and the same measurement resolution and for the no-tolerance case).

The approaches can be treated as a library of self-testing methods. Hence, the designer has the possibility of choice of the self-test method which better fits in the existing hardware of the designed electronic embedded system and better fulfils design assumptions.

It is important to underline the fact that the presented new approach is better when the control unit represented in the paper by the microcontroller has no internal ADC (e.g. the still very popular microcontroller 80C51/52) and better measurement resolution is needed (the internal ADCs based on the SAR method have only 8- or 10-bit resolution with 1.5-bit accuracy). Recently, every microcontroller has at least one 16-bit timer. It works with the precision of the crystal oscillator supplying the microcontroller.

2.1. Idea of the method

The responses of a linear electronic circuit to a square impulse for the assumed range of change of elements for different elements do not fall on each other, as shown in Fig. 2 and explained in [19,20]. Therefore it is possible to discern and to assign these responses to given elements and to their given values. Fig. 2 shows time responses of the analog circuit (shown in Fig. 1) for element value changes from $0.1p_{i\ nom}$ to $5p_{i\ nom}$, (where $p_{i\ nom}$ – nominal value of the i-th element and i=1,..,I, I - the number of elements of the analog part: R_1 – 1st element, R_2 – 2nd element, C_1 – 3rd element, C_2 –4th element for the analog part from Fig. 1).

However, Fig. 3 presents timings on the responses of the analog part for 0.2 nominal values of R_1, C_1 and C_2 elements and timings on outputs of respective comparators: V_1 for the 1st comparator with threshold voltage $v_1 = 0.5$ V, V_2 for the 2nd comparator with $v_2 = 1$ V.

It is seen from Fig. 3 that for each element the output signals from individual comparators are different. They have different duration times τ_k^i according to the value of the i-th element and the value v_k of the threshold voltage of the k-th analog comparator. So we can assign these duration times $\{\tau_k^i\}_{k=1,..,K,\ i=1,..,I}$ of output signals $\{V_k\}_{k=1,..,K}$ to the given values of the particular elements, where K=2.

Fig. 4 shows charts of changes of duration times $\{\tau_k^i\}_{k=1,..,K,\ i=1,..,I}$ of the output signals of the particular comparators in function of changes of the elements' values from 0.1 to 10 $p_{i\ nom}$ depending on two values of the threshold voltages. It is seen that particular charts for the same elements for different threshold voltages (from different outputs of the comparators) and especially charts for different elements are separated. Thus we can make the following assumptions: that the duration time of the output signal of

the 1st comparator τ_1 at the threshold voltage v_1 is the first coordinate, the duration time of the output signal of the 2nd comparator τ_2 at the threshold voltage v_2 is the second one. By successively changing the value p_i of the i-th element from $0.1p_{i\,nom}$ to $10p_{i\,nom}$, the i-th curve is drawn in the measurement K-dimensional (K-D) space. In this way for all I elements and $K = 2$ we obtain a family of localization curves placed on the plane as shown in Fig. 5.

We can present the above operation in the form of the transformation [19]:

$$T_i(p_i) = \sum_{k=1}^{K} \tau_k^i(p_i, v_k)\mathbf{i}_k \tag{1}$$

where: $\mathbf{i}_k$ - is a coordinate vector along the k-axis, k=1, .., K, K – the number of analog comparators, $\tau_k^i(p_i, v_k)$ – the value τ_k^i of the duration time of the output signal of the k-th analog comparator at the threshold voltage v_k for the p_i value of the i-th element.

Thus, we can say that the each curve describes the behavior of the circuit following from a deviation of value of the particular element. Additionally, we can say that using transformation (1) we transform or compress the sets of time responses shown in Fig. 2 to the family of localization curves (Fig. 5).

As described in [21,22] and in this case we can illustrate the fault localization in a graphical way. So, the fault localization consists in putting the measurement point denoted as P_{meas} with coordinates (τ_1^{meas}, τ_2^{meas}) into the measurement space $\tau_1 - \tau_2$ (Fig. 5). Appurtenance of the measurement point to the adequate curve locates the faulty element.

2.2. Tolerance case

In practice all elements have tolerances. Hence, taking into account tolerances of non-faulty elements the localization curves become fuzzy and become localization snakes, as shown in Fig. 6. The family of localization snakes was drawn based on the Monte Carlo method with regard to 1% tolerances of resistors and 5% tolerances of capacitors. In this case the 3-D measurement space $\tau_1 - \tau_2 - \tau_3$ (K = 3) was chosen, where the 3rd comparator has the threshold voltage v_3 = 1.5 V.

The nominal area represents the nominal state of the analog circuit for which values of all elements do not exceed assumed values of tolerances. If a measurement point plotted in the measurement space is enclosed in this area, it means that the tested circuit is fault free – this is the fault detection**.**

Each localization snake represents deviations of values of particular elements. If the measurement point is situated inside the i-th localization snake, it indicates that the i-th element is faulty – the fault localization. Obviously, there are areas where localization snakes penetrate themselves (they were named

cluster areas). In this case the measurement point indicates a cluster of faults (an ambiguous group). It is a disadvantage of the input-output diagnostic method for a circuit with component tolerances.

This map of localization snakes will be serviced to create a fault dictionary which will be described in the next chapter.

2.3. Determination of the K number of the comparators

It is known [23] that the number K of measured parameters of the tested circuit needed for correct fault localization, that is the size of the measurement space – in our case the number of analog comparators, should be at least greater by one than the number F of faults which simultaneously can be present in the faulty circuit ($K \geq F + 1$). Because in the paper single faults were assumed, $F = 1$ (the most common case), the minimal size of the measurement space is equal to 2 ($K = 2$).

There are two opposed ways of determination of the number K. In the first case, we take into account the design of the BIST. It should be as simple as possible. So, it should be built with the smallest number of analog comparators. In this approach also the size of the fault dictionary, which linearly depends on the number K, is the smallest. It is very profitable, because the fault dictionary and codes of measurement and fault diagnosis should occupy a small place in the not great program memory (typically 8, 16 or 32 kB) of the popular 8-bit microcontrollers mainly designed for the main program controlling the embedded system.

In the second case, increment of the number K above $F + 1$ leads to an improvement of fault localization resolution. It follows from the fact that enlargement of the size of the measurement space implies increasing distances between localization curves [21], that is between localization snakes, so they are “more separated”. Thanks to this, the cluster areas are decreased, what enables to localize faults more unambiguously. An increase of the localization resolution is more effective for small K, because if the number K is larger, we have more values of threshold voltages in an admissible voltage range; that is the values of threshold voltages themselves differ less, what gives more and more similar responses at the outputs of next comparators – smaller and smaller differences between duration times of responses at the outputs of neighbouring comparators: $K \to \infty$, $v_{k+1} - v_k \to 0$ and $\tau_{k+1}{}^i - \tau_k{}^i \to 0$.

Taking the above considerations into account, the number K should not be big. For the single fault case, $K = 2, .., 6$ is suggested. This number is obviously dependent on the topology of the tested circuit. It should be small, but enabling correct fault localization at the required level.

For the example circuit (Fig. 1) $K = 3$ was chosen. This number leads to correct fault localization for this circuit (see Fig. 6) and we can present the measurement space in a simple and clear way on a plane, what improves the clarity of description of the presented method.

2.4. Assignment of signal parameters.

The shape of the curves and their mutual locations depend on the duration time of the stimuli and the threshold voltages of the analog comparators.

The way of determination of the duration time T of the stimulating square impulse is described in [20]. In the first step this time is set to a value $1/f_c$, where f_c is the cut-off frequency of the analog part. Next we fit this time in a simulated way to obtain a given maximum value of the signal at the output of the analog part.

We assumed that the threshold voltages should be chosen in a way enabling the best localization resolution of the faults, that is, the localization curves should have similar length and they should be as distant between themselves as possible.

Fig. 7 illustrates changes of the duration time τ^i as a function of changes of element values $p_i/p_{i\,nom}$ and as a function of changes of values of the threshold voltage v.

When the threshold voltage v is higher than the maximum value of the response signal of the analog part, we have areas for which $\tau^i = 0$, as shown in Fig. 7. Thus, we have to choose such values of threshold voltages v for which, in a possibly complete range of changes of element values, the duration time for each element is larger than zero.

In this aim the coefficient Φ_i was introduced [19]:

$$\Phi_i(v) = \bigcup_{l=1}^{L} \operatorname{sgn}(\tau^i(p_{il}, v)) \tag{2}$$

where p_{il} is a discrete value of i-th element and $l = 1, .., L$, L is the number of discrete values of i-th element within a range from $0.1p_{i\,nom}$ to $10p_{i\,nom}$ (each i-th curve is represented by a set of L p_{il} points calculated from p_{il} values based on (1)).

If the $\Phi_i = 1$ (Fig. 8), it means that for the whole range of changes of i-th element values for the given threshold voltage v the duration time $\tau^i > 0$. So, this coefficient is used to choose properly the range of the threshold voltages (it was assumed from 0V to $v_{max} = 1.5$ V). Hence, for the tested analog part (Fig. 1) the threshold voltages v_1 and v_2 were set in a range to 1V and voltage v_3 was established as 1.5V. In the first

and the second case the full range of changes of all element values is mapped onto τ_1 and τ_2 coordinates of the map of localization snakes. In the third case only the τ_3 coordinate for snakes of R_1 and C_2 elements is modified in the full range. This coordinate varies also for element C_1 (Fig. 6).

To determine concrete values $\{v_k\}_{k=1,..,K}$ of the threshold voltages for which we obtain the best localization resolution, a coefficient of localization resolution λ_i of the *i*-th element was introduced:

$$\lambda_i(v) = \max_{l=1,..,L}\{\tau^i(p_{il}, v)\} - \min_{l=1,..,L}\{\tau^i(p_{il}, v)\} \tag{3}$$

where $v \in < 0, v_{max} >$, v_{max} – the maximum value of the assumed range of the threshold voltages.

This coefficient describes the difference between the maximum and minimum value of the duration time τ^i of the circuit response for the given threshold voltage v for a defined range of values of *i*-th element.

The coefficient λ has the form:

$$\lambda(t) = \frac{1}{I}\sum_{i=1}^{I}\frac{\lambda_i(t)}{\max_{k=1,..,K}\{\lambda_i(t)\}} \tag{4}$$

The coefficient λ is an average value of normalized coefficients λ_i, then its maximum value represents the optimum sensitivity of the circuit response to changes of values of all elements. Fig. 9 shows the coefficients λ_i of all elements and the coefficient λ.

Based on this coefficient and earlier established ranges of threshold voltages and also the fact that values of threshold voltages should possibly differ as much as possible between themselves and be higher than the "0" digital signal (160mV for the Atmega16), the following values of voltages were established: v_1 = 0.5V, v_2 = 1V and v_3= 1.5V. For these values Fig. 5 and Fig. 6 were drawn.

3. THE FAULT DIAGNOSIS PROCEDURES

We can distinguish the following fault diagnosis procedures:

- Creation of the fault dictionary realized during the design of the embedded system and only once for a given analog circuit by the personal computer.
- The measurement procedure, where the BIST consisting of analog comparators and peripherals of the microcontroller obtains information about the tested circuit, and the microcontroller controls this procedure according to the measurement function included in its program memory.

- The fault detection and localization procedure elaborated to detect and to localize single soft faults of passive elements in the tested analog circuit.

Two last procedures are run during self-testing of the embedded system.

3.1. The fault dictionary creation procedure

From Fig. 6 it can be seen that the fault dictionary should contain a description of the nominal area and descriptions of particular localizations snakes. So, generation of the fault dictionary was divided into two stages. In the first stage the data describing the nominal area are created, and in the second one data represent the individual localization snakes.

It was assumed that values of time τ_1, τ_2, and τ_3 have a form compatible with the data format of the 16-bit Timer 1 of the microcontroller, that is they are integer 16-bit numbers with a range from 0000h to FFFFh. Thanks to this fact, the results of times measured by the Timer 1 can be directly compared with the fault dictionary.

We decided to approximate the nominal area by a *K*-dimensional ellipsoid, because it better approximates this area (it better "fits" this area) than a *K*-dimensional sphere. In the paper we present the methodology of creation of the ellipsoid on an example of a spheroid for K=3, because the spheroid is obtained by rotating an ellipse about one of its axes and we can describe the ellipse only by coordinates of its focuses F_1 and F_2 and the length $2a$ of the major axis. This description is ideally suitable for a fault detection algorithm, because we need to test that the sum of two distances between the measurement point P_{meas} and individual focuses F_1 and F_2 of the ellipse is not greater than the length $2a$ of the major axis. This solution does not need complex calculations, so it can be boldly implemented in microcontrollers which have no big computing power.

Determination of parameters of the approximation spheroid is realized by the following algorithm:

- M points with coordinates (τ_1^m, τ_2^m, τ_3^m) representing the nominal area are generated using the Monte Carlo method, where $m = 1, .., M$.
- Based on these points, coefficients A_1, A_2, B_1, B_2 of the approximation straight line of the nominal area given by a formula $\tau_2 = A_1 \cdot \tau_1 + A_2$; $\tau_3 = B_1 \cdot \tau_1 + B_2$ are determined. This line passes through the nominal point P_{nom} with coordinates (τ_1^{nom}, τ_2^{nom}, τ_3^{nom}). Its coefficients are calculated using the *polifit* function of Matlab.
- Next, angles of inclinations of the approximation straight line (simultaneously angles of inclinations of the approximation spheroid) are calculated: the angle of inclination between the straight

line $\tau_2 = A_1 \cdot \tau_1$ placed on the plane $\tau_1 - \tau_2$ and the τ_1 axis $\phi_1 = \text{arc tang}(A_1)$, the angle of inclination between the straight line $\tau_3 = B_1 \cdot \tau_1$ placed on the plane $\tau_1 - \tau_3$ and the τ_3 axis $\phi_2 = \text{arc tang}(B_1 \cdot \cos(\phi_1))$

- The nominal area (the set of M points) $\{(\tau_1^m,\ \tau_2^m,\ \tau_3^m)\}_{m=1,..,M}$ is moved over by the vector $[-\tau_1^{nom}, -\tau_2^{nom}, -\tau_3^{nom}]$. Next, this set is rotated about angles ϕ_1 and ϕ_2:

$$\begin{aligned} \tau_1^{m,r} &= (\tau_1^m \cdot \cos(\phi_1) + \tau_2^m \cdot \sin(\phi_1)) \cdot \cos(\phi_2) + \tau_3^m \cdot \sin(\phi_2) \\ \tau_2^{m,r} &= -\tau_1^m \cdot \sin(\phi_1) + \tau_2^m \cdot \cos(\phi_1) \\ \tau_3^{m,r} &= -\tau_1^m \cdot \sin(\phi_2) + \tau_3^m \cdot \cos(\phi_2) \end{aligned} \tag{5}$$

  In this way we get the new set of points $\{(\tau_1^{m,\mathrm{r}},\ \tau_2^{m,\mathrm{r}},\ \tau_3^{m,\mathrm{r}})\}_{m=1,..,M}$ which can be approximated by a spheroid with the centre (0,0,0) and focuses placed on the τ_1 axis. It enables to use basic formulas for the calculation of parameters of the ellipse creating the spheroid by rotation.

- Lengths of major $2a$ and minor $2b$ axes of the ellipse are determined from relationships:

$$\begin{aligned} a &= (\max_{m=1,..,M}\{\tau_1^{m,r}\} - \min_{m=1,..,M}\{\tau_1^{m,r}\})/2 \\ b &= (\max\{(\max_{m=1,..,M}\{\tau_2^{m,r}\} - \min_{m=1,..,M}\{\tau_2^{m,r}\}), (\max_{m=1,..,M}\{\tau_3^{m,r}\} - \min_{m=1,..,M}\{\tau_3^{m,r}\})\})/2 \end{aligned} \tag{6}$$

- Next, we calculate distances between focuses and the centre of the ellipse: $c = \sqrt{a^2 + b^2}$
- At the end, coordinates of focuses $\mathrm{F}_1(\tau_1^{\mathrm{F1}},\ \tau_2^{\mathrm{F1}},\ \tau_3^{\mathrm{F1}})$ and $\mathrm{F}_1(\tau_1^{\mathrm{F2}},\ \tau_2^{\mathrm{F2}},\ \tau_3^{\mathrm{F2}})$ of the spheroid are calculated from formulas:

$$\begin{cases} \tau_1^c = c \cdot \cos(\phi_1) \cdot \cos(\phi_2) \\ \tau_2^c = c \cdot \sin(\phi_1) \cdot \cos(\phi_2) \\ \tau_3^c = \sin(\phi_2) \end{cases} \tag{7}$$

and

$$\begin{cases} \tau_1^{F1} = \tau_1^{nom} + \tau_1^c \\ \tau_2^{F1} = \tau_2^{nom} + \tau_2^c \\ \tau_3^{F1} = \tau_3^{nom} + \tau_3^c \end{cases} \qquad \begin{cases} \tau_1^{F2} = \tau_1^{nom} - \tau_1^c \\ \tau_2^{F2} = \tau_2^{nom} - \tau_2^c \\ \tau_3^{F2} = \tau_3^{nom} - \tau_3^c \end{cases} \tag{8}$$

The approximation straight line and the approximation spheroid are shown in Fig. 10. The spheroid is a graphical representation of the fragment of the fault dictionary used during the fault detection procedure.

Because the described self-testing method is implemented in 8-bit microcontrollers, which do not have big computing power, the taxi norm to calculate distances between points in the fault detection and localization algorithm was assumed. It considerably simplifies calculations, because we use only three integer operations: a subtraction, an absolute value and an addition. Hence the coefficient $2a$ (the length of the major axis) was replaced by the equivalent coefficient $e = 2(c + b)$

The following parameters in the form of words (two bytes) of the approximation spheroid are written to the fault dictionary: $\{(\tau_1^{F1}, \tau_2^{F1}, \tau_3^{F1}), (\tau_1^{F2}, \tau_2^{F2}, \tau_3^{F2}), e\}$

It was assumed that each localization snake is described by the localization curve from which it was created by fuzziness of this curve by taking into account tolerances of no-fault elements as well as by the coefficient ξ_i representing half of the diameter of the i-th snake.

The i-th localization curve can be presented as a set of coordinates $\{(\tau_1^{il}, \tau_2^{il}, \tau_3^{il})\}_{l=1,..,L}$ of L points p_{il} evenly placed on it. So, if we take into account the above assumptions, the i-th localization snake is described by the set of L spheres $\{S_{il}\}_{l=1,..,L}$ with centres in points p_{il} and the radius ξ_i as was shown in Fig. 11. Hence the closeness of placement of the spheres decides about exactitude of approximation of the snake. The more the closeness the better the approximation of the snake, but the size of the fault dictionary becomes greater and greater. We are anxious about it that the size of the fault dictionary should be possibly the smallest, because the fault dictionary and codes of self-testing procedures should leave more place for the main application in the not big program memory of the microcontroller.

A better solution is to replace spheres by cylinders with a radius ξ_i. It better approximates the localization snake, but the calculations are considerably more complicated. In the first step we have to assign formulas $\frac{\tau_1 - \tau_1^{il}}{C_1^{ij}} = \frac{\tau_2 - \tau_2^{il}}{C_2^{ij}} = \frac{\tau_3 - \tau_3^{il}}{C_3^{ij}}$ of straight lines passing through points p_{il} and $p_{i(l+1)}$ l=1, .., L - 1 in a three-dimensional (3-D) space and to remember these coefficients, where $C_k^{ij} = \tau_k^{i(l+1)} - \tau_k^{il}$ and k = 1, 2, 3. But, during the localization algorithm we have to calculate $I \cdot L$ distances d_{il} between the measurement point P_{meas} $(\tau_1^{meas}, \tau_2^{meas}, \tau_3^{meas})$ and these approximation lines based on a complex relation:

$$d_{il} = \frac{\left|(\tau_1^{meas} - \tau_1^{il}) \cdot C_2^{il} - (\tau_2^{meas} - \tau_2^{il}) \cdot C_1^{il}\right| + \left|(\tau_2^{meas} - \tau_2^{il}) \cdot C_3^{il} - (\tau_3^{meas} - \tau_3^{il}) \cdot C_2^{il}\right|}{\left|C_1^{il}\right| + \left|C_2^{il}\right| + \left|C_3^{il}\right|} + \\ + \frac{\left|(\tau_3^{meas} - \tau_3^{il}) \cdot C_1^{il} - (\tau_1^{meas} - \tau_1^{il}) \cdot C_3^{il}\right|}{\left|C_1^{il}\right| + \left|C_2^{il}\right| + \left|C_3^{il}\right|} \tag{9}$$

It is seen (9) that additionally we have to use multiplication and division operations and the result should be in a floating format, which considerably increases total calculation time and size of the code of the localization procedure.

For the approach based on spheres we calculate only distances between the measurement point P_{meas} and particular points p_{il} (centres of spheres S_{il}) from a simple relation:

$$d_{il} = \left|\tau_1^{meas} - \tau_1^{il}\right| + \left|\tau_2^{meas} - \tau_2^{il}\right| + \left|(\tau_3^{meas} - \tau_3^{il})\right| \tag{10}$$

We finally decided to approximate the localization snake by spheres. But, the following assumptions were made:

- The i-th localization curve is described by the coordinates (τ_1^{i1}, τ_2^{i1}, τ_3^{i1}) of starting point p_{i1} and a set of vectors $\{\mathbf{q}_{il}\}_{l=1,\ ..,\ L-1}$, where $\mathbf{q}_{il}$ has coordinates [$\tau_1^{il,q}$, $\tau_2^{il,q}$, $\tau_3^{il,q}$], where $\tau_1^{il,q} = (\tau_1^{i(l+1)} - \tau_1^{il})/\rho$, $\tau_2^{il,q} = (\tau_2^{i(l+1)} - \tau_2^{il})/\rho$, $\tau_3^{il,q} = (\tau_3^{i(l+1)} - \tau_3^{il})/\rho$. That is, all points p_{il} are obtained from successive movements of the starting point p_{i1} about successive vectors $\mathbf{q}_{il}$. Lengths of vectors $\mathbf{q}_{il}$ (distances between next points of the curve) should not be greater than $2\cdot\xi_i$ to correctly approximate the i-th localization snake.
- The coefficient ρ represents additional concentration of spheres between two ones S_{il} and $S_{i(l+1)}$. It enables to improve the exactitude of approximation of the snake without enlargement of the size of the fault dictionary. In this way we improve the fault localization closeness σ, which can be graphically expressed by division of the volume of a fragment of the sphere with radius ξ_i contained in the cylinder by the volume of this cylinder with radius ξ_i and a height $h_i \le \xi_i$ (Fig. 12):

$$\sigma = \frac{V_{fragment\ of\ sphere}}{V_{cylinder}} = \frac{\left(6\xi_i^2 - 2h_i^2\right)}{6\xi_i^2} = \frac{\left(6\left(\frac{\xi_i}{h_i}\right)^2 - 2\right)}{6\left(\frac{\xi_i}{h_i}\right)^2} = \frac{\left(6\rho^2 - 2\right)}{6\rho^2} \tag{11}$$

Fig. 13 shows the graph of the coefficient σ in function of the coefficient $\rho = \xi_i./\ h_i$. It is seen that triple and especially quadruple concentration of spheres gives good, satisfying fault localization closeness σ at a level higher than 0.97. So we assumed $\rho = 4$.

Assignment of coefficients ξ_i representing half of the diameters of the respective fragments of snakes included in the nominal area, that is coefficients of belonging of the measurement points to respective snakes, is realized by the algorithm which consists of the following steps:

- M points $\{p_{ilm}\}_{m=1,\ ..,\ M}$ with coordinates (τ_1^{ilm}, τ_2^{ilm}, τ_3^{ilm}) around the point p_{il} are generated using the Monte Carlo method, where point $p_{i(l-1)}$ is the nominal point P_{nom} (τ_1^{nom}, τ_2^{nom}, τ_3^{nom}).
- An unit vector $\mathbf{u}_{il}$ [$\tau_1^{il,u}$, $\tau_2^{il,u}$, $\tau_3^{il,u}$] passing through the points P_{nom} and p_{il} is calculated:

$$\begin{cases} \tau_1^{il,u} = \left(\tau_1^{il} - \tau_1^{nom}\right)/E^{il} \\ \tau_2^{il,u} = \left(\tau_2^{il} - \tau_2^{nom}\right)/E^{il} \\ \tau_3^{il,u} = \left(\tau_3^{il} - \tau_3^{nom}\right)/E^{il} \end{cases} \quad \text{and} \quad E^{il} = \sqrt{\left(\tau_1^{il} - \tau_1^{nom}\right)^2 + \left(\tau_2^{il} - \tau_2^{nom}\right)^2 + \left(\tau_3^{il} - \tau_3^{nom}\right)^2} \tag{12}$$

- Next, the coefficient D_{il} of the plane Π_{il}: $A_{il}\cdot\tau_1 + B_{il}\cdot\tau_2 + C_{il}\cdot\tau_3 + D_{il} = 0$ orthogonal to the vector $\mathbf{u}_{il}$ and passing through the point p_{il} is calculated (where: $A_{il}\cdot = \tau_1^{il,u}$, $B_{il} = \tau_2^{il,u}$, $C_{il} = \tau_3^{il,u}$):

$$D_{il} = -\left(A_{il}\cdot\tau_1^{il} + B_{il}\cdot\tau_2^{il} + C_{il}\cdot\tau_3^{il}\right) \tag{13}$$

- Projection of all points $\{p_{ilm}\}_{m=1,\ ..,\ M}$ on the plane Π_{il} and next calculation of distances between projected points $\{p^*_{ilm}\}_{m=1,\ ..,\ M}$ for every m are realized in the following way:
  - Determination of the coefficient D_{ilm} of the plane Π_{ilm} passing through the point p_{ilm} and parallel to the plane Π_{il}:

$$D_{ilm} = -\left(A_{il}\cdot\tau_1^{ilm} + B_{il}\cdot\tau_2^{ilm} + C_{il}\cdot\tau_3^{ilm}\right) \tag{14}$$

  - Calculation of distance with the sign d_{ilm} between the point p_{ilm} and the plane Π_{ilm}: $d_{ilm} = D_{ilm} - D_{il}$
  - Determination of the vector $\mathbf{v}_{ilm}$ $[\tau_1^{ilm,v}, \tau_2^{ilm,v}, \tau_3^{ilm,v}]$ (parallel to the vector $\mathbf{u}_{il}$) moving the point p_{ilm} to the plane Π_{il} : $\tau_1^{ilm,v} = \tau_1^{il,u}\cdot d_{ilm}$, $\tau_2^{ilm,v} = \tau_2^{il,u}\cdot d_{ilm}$, $\tau_3^{ilm,v} = \tau_3^{il,u}\cdot d_{ilm}$
  - Movement of the point p_{ilm} to the plane Π_{il}. The projected point p^*_{ilm} has the coordinates: $\tau_1^{ilm,*} = \tau_1^{ilm} + \tau_1^{ilm,v}$, $\tau_2^{ilm,*} = \tau_2^{ilm} + \tau_2^{ilm,v}$, $\tau_3^{ilm,*} = \tau_3^{ilm} + \tau_3^{ilm,v}$
  - Calculation of distances ξ_{im} between the point p^*_{ilm} and the point p_{il}:

$$\xi_{im} = \left|\tau_1^{ilm,*} - \tau_1^{il}\right| + \left|\tau_2^{ilm,*} - \tau_2^{il}\right| + \left|\tau_3^{ilm,*} - \tau_3^{il}\right| \tag{15}$$

- Finally, the coefficient ξ_i of belonging of the measurement point to the i-th snake is determined: $\xi_i = \max_{m=1,..,M}\{\xi_{im}\}$

Hence, the i-th localization snake is described by the set consisting of the description of the i-th localization curve and the range of its fuzziness in the space (half of thickness of the i-th snake): $\{(\tau_1^{i1}, \tau_2^{i1}, \tau_3^{i1}), \{[\tau_1^{il,q}, \tau_2^{il,q}, \tau_3^{il,q}]\}_{l=1,..,L-1}, \xi_i, \rho\}$

So, finally we can describe the fault dictionary in the following way: $F_{IL} = \{(\tau_1^{F1}, \tau_2^{F1}, \tau_3^{F1}), (\tau_1^{F2}, \tau_2^{F2}, \tau_3^{F2}), e, \{(\tau_1^{i1}, \tau_2^{i1}, \tau_3^{i1}), \{[\tau_1^{il,q}, \tau_2^{il,q}, \tau_3^{il,q}]\}_{l=1,..,L-1}, \xi_i\}_{i=1,..,I}, \rho\}$ Hence, the fault dictionary has the dimension $2\cdot(2\cdot K + I\cdot(L+1)\cdot K + 2)$ bytes. When K=3 (I=4, J=32 or J=64) it is still small (808 or 1600 bytes) in relation to the size of the program memory of a typical 8-bit microcontroller (e.g. ATmega16 has 16kB of FLASH memory).

The fault dictionary is generated on a PC computer using the Matlab program with the Control Toolbox, and saved to a text file based on the *dlmwrite* function. Next, it is converted and placed into the file with the full code of a program. This file is compiled to the Intel-HEX file. In the last step the microcontroller is programmed.

3.2. The measurement procedure

This procedure is realized by the measurement microsystem (the BIST) controlled by the microcontroller [19]:

- the microcontroller timers determine the duration time T of the stimuli and they measure duration times $\{\tau_k\}_{k=1,..,K}$ of signals at the outputs of the K comparators,
- the analog comparators with different threshold voltages convert the response signal of the analog part to a square impulse.

The measurement procedure was implemented in the laboratory system (Fig. 14) based on the ATmega16 microcontroller [24]. The 8-bit Timer 2 controls the duration time T of the stimulating square impulse on the OC2 line connected to the input of the tested analog circuit. The 16-bit Timer 1 is responsible for measuring the duration times $\{\tau_k\}_{k=1,..,K}$ of output signals of the comparators. The 12-bit DAC programmable via the SPI interface sets the threshold voltage of the analog comparator. Thanks to this solution we use only one comparator instead of K comparators. This solution is flexible and particularly useful during the testing of the method.

Hence, to measure K duration times we have to repeat the measurement procedure K times. Timings of this procedure are shown in Fig. 15.

First we set a low level at the input of the analog part during time required to introduce the tested circuit to an initial state (it was assumed $8T$). In this time we set the value v_k of the threshold voltage in the output the DAC. After this time the tested circuit is stimulated by the square impulse with the duration time T. Next, at the output of the analog comparator a square impulse appears. Its duration time τ_k is measured by the Timer 1.

This procedure is implemented by the measurement function [19], which the algorithm is shown in Fig. 16. It is realized in the main program and two interrupt services: from the Timer 2 Overflow and the Timer 1 Input Capture. This function is called out with the variable $v[k]$ representing the threshold voltage v_k and it returns the variable $result[k]$ with the measurement duration time τ_k.

We use the variable *end_conv* to synchronize the main function and the interrupt service of Timer 1. The variable *edge* is used to determine an active edge for the Input Capture Circuit of Timer 1. The measurement result of the duration time τ_k is calculated in the Timer 1 Input Capture Interrupt service. The calculations base on values captured from the free-running Timer 1 at moments of active edges of the output signal of the analog comparator and saved in the register ICR1.

Finally, repeating the measurement function three times, we get the measurement result in the form of a two-byte variables table *result*[1], *result*[2], *result*[3], where respective variables contain measurement times τ_1^{meas}, τ_2^{meas}, τ_3^{meas} adequately.

3.3. The fault detection and localization procedure

The microcontroller, based on the measurement point P_{meas} with coordinates (τ_1^{meas}, τ_2^{meas}, τ_3^{meas}) and the fault dictionary F_{IJ} contained in its program memory, realizes the detection and localization of single soft faults of passive elements according to the procedure described bellow.

This procedure is realized by the *fault_diagnosis* function. It was divided into two parts. In the first part the fault detection is performed. In the second one, if a fault is detected, its localization is carried out. The result of the fault diagnosis is kept in the byte variable *fdresult*. A way of coding of respective faults is shown in Fig. 17.

The fault detection bases on checking if the measurement point P_{meas} is contained inside the approximation spheroid described by $\{(\tau_1^{F1}, \tau_2^{F1}, \tau_3^{F1}), (\tau_1^{F2}, \tau_2^{F2}, \tau_3^{F2}), e\}$ For this purpose the following inequality is calculated and tested:

$$\sum_{k=1}^{3}\left(\left|\tau_k^{meas}-\tau_k^{F1}\right|+\left|\tau_k^{meas}-\tau_k^{F2}\right|\right)\le e \tag{16}$$

If the inequality (16) is fulfilled (the measurement point is placed inside the spheroid), the tested analog part is fault-free. The bit *nom* in the variable *fdresult* is set, and the fault diagnosis procedure is finished.

Else the microcontroller runs the fault localization part. For all *I* localization snakes the following fault localization algorithm are realized:

- The distance d_i represented by an element $d[i]$ of the table of the integer variables $d[I]$ between the measurement point P_{meas} and the *i*-th localization curve is determined in the way shown in Fig. 18. At the beginning of the fragment of the localization algorithm the variables $d[i]$, p_{il}^{ρ}, l are initialized. Two points p_{il}^{ρ} with coordinates ($\tau_1^{il,\rho}$, $\tau_2^{il,\rho}$, $\tau_3^{il,\rho}$) and P_{meas} represent *K*-dimension tables (*K*=3) of coordinates *p_ilr*[*K*] and *p_meas*[*K*] adequately. Next $P \cdot L$ times (*P*=4 and *L*=64) the distance between the measurement point P_{meas} and the successive point p_{il}^{ρ} represented the *i*-th curve based on the *distance* function is calculated, which realizes the relationship (17) and the result returns to the temporary variable *d_t*:

$$d_t = \sum_{k=1}^{K} \left| \tau_k^{il,\rho} - \tau_k^{meas} \right| \tag{17}$$

Then the point p_{il}^{ρ} is moved to the next position by the vector $\mathbf{q}_{il}$ described by the table $q\_il[K]$. This operation is realized by the *move* function. After this operation the content of the variable $d[i]$ is compared with the content of the temporary variable d_t. If the value of the d_t is smaller than the value of the $d[i]$, the variable $d[i]$ is actualized by the value of the d_t, because we assumed that the smaller distance from all distances d_{il}^{ρ} between P_{meas} and all p_{il}^{ρ} represents the distance d_i between the point P_{meas} and the i-th curve: $d_i = \min_{l=1,..,L} \left\{ \min_{\rho=1,..,P} \left\{ d_{il}^{\rho} \right\} \right\}$ So, we realize the $min\{\cdot\}$ function in a simple way using only one integer variable. Finishing this fragment of the localization algorithm the variable $d[i]$ keeps the distance d_i between the measurement point P_{meas} and i-th localization curve.

- In the last step of the algorithm, inequality $d_i < \xi_i$ is tested. If this relationship is fulfilled, the bit representing a failure of the i-th element (see Fig. 17) is set in the variable *fdresult*.

Hence, after finishing the fault localization algorithm, in the variable *fdresult* one bit unambiguously indicating the faulty element of the tested circuit can be set, or the *nom* bit representing a nominal state of the circuit, or more bits. In this case these bits represent a cluster of faults. It is caused by mutual penetration of localization snakes, what makes impossible to point to a concrete fault, only to point to a group of elements from which one is faulty. If any bit of the variable *fdresult* is not set, it means that there are multiple faults in the tested circuit.

At the end of self-testing of the analog part, when the fault is detected, the embedded system should enter the alarm state, and the fault localization results should be e.g. transmitted to the personal computer or they should be displayed on any display mounted in the system.

4. EXPERIMENTAL VERIFICATION

The new fault diagnosis method was experimentally verified on the example of the low-pass filter shown in Fig. 14. The picture of the laboratory system is shown on Fig. 19. The tested analog part consists of an operational amplifier NE5534 of Texas Instruments operating from a double power supply (V_- = -12 V, V_+ = +12 V), two resistors $R_1 = R_2 = 10$ kΩ and two capacitors $C_1 = 10.03$ nF and $C_2 = 21.41$ nF. It is tested by the digital part represented by the ATmega16 (Fig. 19). It works with a 4 MHz quartz crystal oscillator. Timer 1 is clocked directly by the system clock. It is used to determine the duration times τ_1, τ_2, τ_3. Timer 2, clocked by the system clock with the prescaler divisor 8, generates

at the output OC2 stimulating square impulses with a duration time $T = 500$ μs and with an amplitude equal to $V_{cc} = 5$ V. The threshold voltages are set: $v_1 = 0.5$ V (a value 0x19B loaded to the external DAC MAX5352 by the reference voltage $V_{ref} = 5$ V), $v_2 = 1$ V (a value 0x335) and $v_3 = 1.5$ V (a value 0x4D0) and verified by the multimeter HP34401A.

Measurements were carried out for 33 values of each element. One value was set to the nominal value and the 32 values were logarithmically located in the following ranges of element value changes: from 100 Ω to 100 kΩ for R_1 and R_2, from 1.1 nF to 1100 nF for C_1 and from 2.2 nF to 220 nF for C_2.

Different soft faults of each *i*-th element were physically entered to the analog part and diagnosed on the level of fault detection and localization. For resistors a decade resistor was used and for the capacitors a decade capacitor whose values were controlled by the impedance analyzer HP4192A. To verify the measurement procedure and correctness of work of the BIST, the microcontroller measured times τ_1^{meas}, τ_2^{meas}, τ_3^{meas} and next it sent them to the personal computer via the RS232.

In theoretical considerations and Matlab's simulations we assumed that the operational amplifier and the analog comparator are ideal. In practice they have real parameters. Additionally, the digital output OC2 of the microcontroller does not generate an ideal square impulse, but an impulse with the voltage offset of about 160 mV and rise and fall times depending on the load [24]. So, the experimental results were finally used to correct the fault dictionary.

An example of experimental results is shown in Table 1. It only concerns the results of localization of the C_1 element made by the fault diagnosis algorithm. Table 1 shows also coordinates of the respective measurement points and the symbol of the element or symbol of the cluster qualified as faulty.

The localization curves based on the experimental results and the measurement points in the form of symbols representing deviations of values of particular elements are shown in Fig. 20.

Comparing Fig. 20 with experimental curves and Fig. 6 with theoretical snakes it is seen that the placement and shape of the respective curves and snakes are similar, in spite of the fact that a simple model was used in the simulation, without taking into account the parameters of active elements of the analog part. The experimental results show that the method works correctly and (based on the fault dictionary corrected by experimental results) it can be implemented with success for testing or self-testing of the analog part with component tolerances of mixed-signal embedded systems controlled by the microcontrollers.

5. CONCLUSIONS

A new approach to self-testing of analog parts of electronic embedded systems based on using the peripheral devices of the control unit, especially microcontrollers, controlling the electronic embedded systems to create the reconfigurable measurement microsystems (BISTs) is proposed in the paper. Also a new input-output fault diagnosis method of analog circuits assembled on a printed circuit board with component tolerances was presented in the paper. The method can be also used for the parametric identification of technical or biomedical objects modelled by electrical circuits. This approach also can be useful for self-testing of mixed-signal systems on a chip (SoC).

The important advantage of this approach is the fact that the BIST additionally needs only a few analog comparators, because its remaining elements are included in the microcontroller controlling the embedded system, which simplifies its structure, i.e. decreases test costs. Also the use of the microcontroller to create and to control the BIST increases its flexibility and functionality.

This fault diagnosis method was elaborated for the fault diagnosis of analog parts of electronic embedded systems controlled by control units with moderate computing power (e.g. 8-bit microcontrollers), therefore the method has the following advantages:

- The tested analog part is stimulated by a digital signal directly generated by a digital part and its final response also has the form of a digital signal. So the digital part can generate a stimulus and receive the response of the analog part.
- Exclusively internal resources of popular microcontrollers (timers) and analog comparators are used to measure parameters of analog parts.
- The algorithm of the fault diagnosis procedure is simple in spite of the fact that we diagnose a circuit with component tolerances, and the calculations made in the diagnosis procedure base on only integer instructions. Hence the diagnosis procedure does not require big computing power. Thus, this method can be used by typical 8-bit microcontrollers.
- The size of the codes of the measurement and diagnosis procedures and the size of the code of the fault dictionary are small. Thus, these codes can be added to the main program controlling the embedded system without the risk of exceeding the program memory size of the microcontroller.

REFERENCES

[1] Zhao F., Koutsoukos X., Haussecker H., Reich J., Cheung P.: Monitoring and fault diagnosis of hybrid systems. IEEE Transactions on Systems, Man, and Cybernetics—Part B: Cybernetics, Vol. 35, No. 6, December 2005, pp. 1214-1219.

[2] Scottow R. G., Hopkins A. B. T.: Instrumentation of real-time embedded system for performance analysis, in: Proceedings of IEEE Instrumentation and Measurement Conference, IMTC/06, Sorrento, Italy 24-27 April, 2006, pp. 1307-1310.

[3] Changhyun B., Seungkyu P., Kyunghee C.: [similar to] TEST: An effective automation tool for testing embedded software, WSEAS Transactions on Information Science and Applications, Vol. 2, no. 8, August, 2005, p 1214-1219.

[4] Souza C. P., Assis F. M., Freire R. C. S.: Mixed test pattern generation using single parallel LFSR. in: Proceedings of IEEE Instrumentation and Measurement Conference, IMTC/06, Sorrento, Italy 24-27 April, 2006, pp. 1114-1118.

[5] Ehsanian M., Kaminska B., Arabi K.: A new on-chip digital BIST for analog-to-digital converters, Microelectronic Reliability, Vol. 38, No. 3, 1998, pp. 409-420.

[6] Vecera I., Vrba R.: An algorithmic A/D switched-current converter for smart signal digitization with self-test features, Measurement 35 (2) (2004) 153-160.

[7] Chen H., Vivek Chandrasekhar V., Yelamarthi K.: Low-Cost Low-Power Self-Test Design and Verification of On-Chip ADC for System-on-a-Chip Applications, in: Proceedings of IEEE Instrumentation and Measurement Conference, IMTC/06, Sorrento, Italy, April 2006, pp. 1301-1306.

[8] Venuto D., Reyneri L.: Fully digital strategy for fast calibration and test of SD ADCs, Microelectronic Journal 38 (4-5) (2007) 474-481.

[9] Yun-Che W., Kuen-Jong L.: A current-mode BIST structure of DACs, Measurement 31 (3) (2002) 147-163.

[10] Raczkowycz J., Mather P., Saine S.: Using a sigma-delta modulator as a test vehicle for embedded mixed-signal test, Microelectronic Journal 31 (8) (2000) 689-699.

[11] Prenat G., Mir S., Vazques D., Rolindez L.: A low-cost digital frequency testing approach for mixed-signal devices using ΣΔ modulation, Microelectronic Journal 36 (12) (2005) 1080-1090.

[12] Arabi K., Kamińska B.: Design for Testability of Embedded Integrated Operational Amplifiers, IEEE Journal of Solid-State Circuits, Vol. 33, No. 4, April 1998, pp. 573-581.

[13] Arabi K., Kamińska B.: Oscillation-Test Methodology for Low-Cost Testing of Active Analog Filters, IEEE Transactions on Instrumentation and Measurement 48 (4) (1999) 798-806.

[14] Toczek W., Zielonko R.: A measuring systems for fault detection via oscillation, in: Proceedings of XVI IMEKO World Congress, Vienna, Austria, 2000, vol. 6, pp. 287-292.

[15] Lubaszewski M., Mir S., Kolarik V., Nielsen Ch., Courtois B.: Design of Self-Checking Fully Differential Circuits and Boards, IEEE Transactions on Very Large Scale Integration (VLSI) Systems, vol. 8, no. 2, April 2000, pp. 113-127.

[16] Toczek W.: Analog fault signature based on sigma-delta modulation and oscillation - test methodology, Metrology and Measurement Systems, Vol. XI, No. 4, 2004, pp. 363-375.

[17] Huertas G., Vazques D., Peralias E., Rueda A., Huertas J. L.: Oscillation-based test in oversampled ΣΔ modulators, Microelectronic Journal 33 (10) (2002) 799-806.

[18] Negreiros M., Carro L., Susin A. A.: Testing analog circuits using spectral analysis, Microelectronic Journal 34 (10) (2003) 937-944.

[19] Czaja Z.: A fault diagnosis method of analog electronic circuits for mixed-signal systems controlled by microcontrollers, in: Proceedings of IEEE Instrumentation and Measurement Conference, IMTC/06, Sorrento, Italy, April 2006, pp. 1211-1216.

[20] Czaja Z.: A diagnosis method of analog parts of mixed-signal systems controlled by microcontrollers, Measurement 40 (2) (2007) 158-170.

[21] Czaja Z., Zielonko R.: On fault diagnosis of analogue electronic circuits based on transformations in multi-dimensional spaces, Measurement 35 (3) (2004) 293-301.

[22] Czaja Z., Zielonko R.: Fault diagnosis in electronic circuits based on bilinear transformation in 3D and 4D spaces, IEEE Transaction on Instrumentation and Measurement 52 (1) (2003) 97-102.

[23] Liu R.: Testing and diagnosis of analog circuits and systems, Van Nostrand Reinhold, USA, New York, 1991.

[24] Atmel Corporation: 8-bit AVR microcontroller with 16k Bytes In-System Programmable Flash, ATmega16, ATmega16L, PDF file, 2003, Available from: <www.atmel.com>.

Table 1. An example of experimental results of localization of the C_1 element made by the fault diagnosis algorithm.

C_1[nF]	τ_1 [*0.25μs]	τ_2 [*0.25μs]	τ_3 [*0.25μs]	**Localisation result**
2.20	3755	3061	2626	C_1
3.44	3704	3031	2608	C_1
4.62	3655	3001	2592	C_1
7.22	3554	2951	2570	C_1
9.72	3458	2918	2562	C_1
15.17	3345	2906	2579	(R_1,R_2,C_1)
22.00	3342	2951	2633	nominal
31.89	3452	3069	2744	C_1
49.80	3736	3327	2972	C_1
67.03	4020	3572	3185	C_1
104,67	4613	4075	3608	C_1
140.89	5167	4477	3941	C_1
220.00	6499	5220	4538	C_1

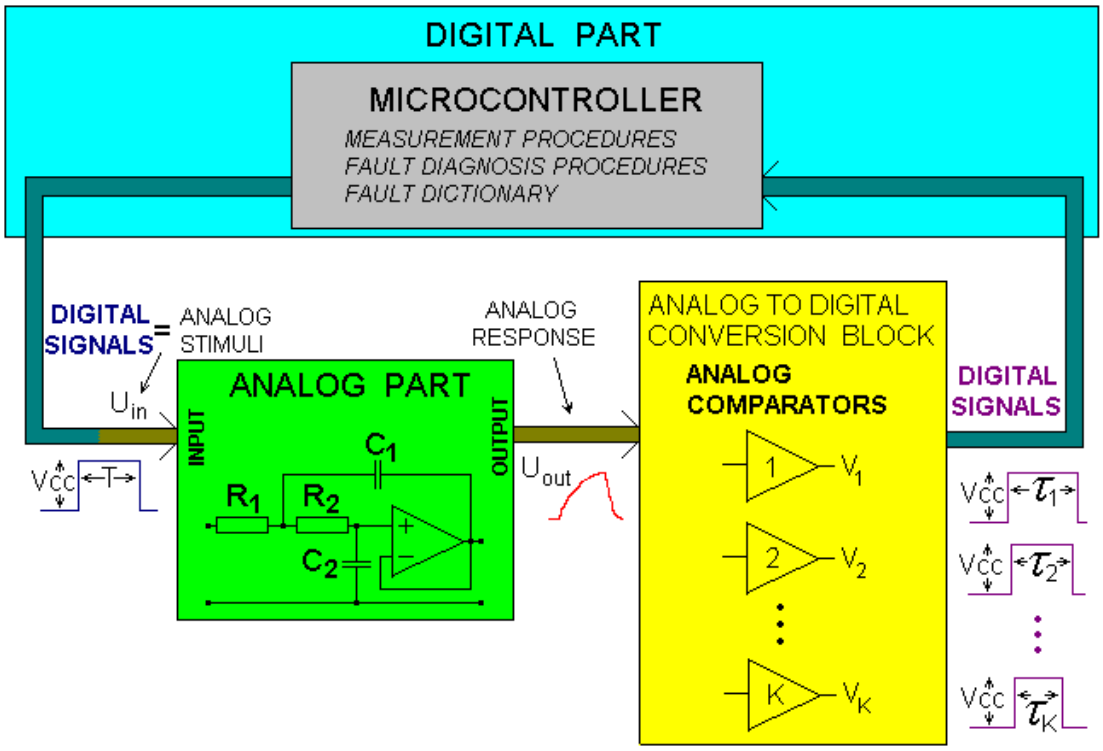

Fig. 1. Mixed-signal electronic system controlled by the microcontroller with self-testing of the analog part (where: $R_1 = R_2 = 10$ kΩ, $C_1 = 11$ nF, $C_2 = 22$ nF)

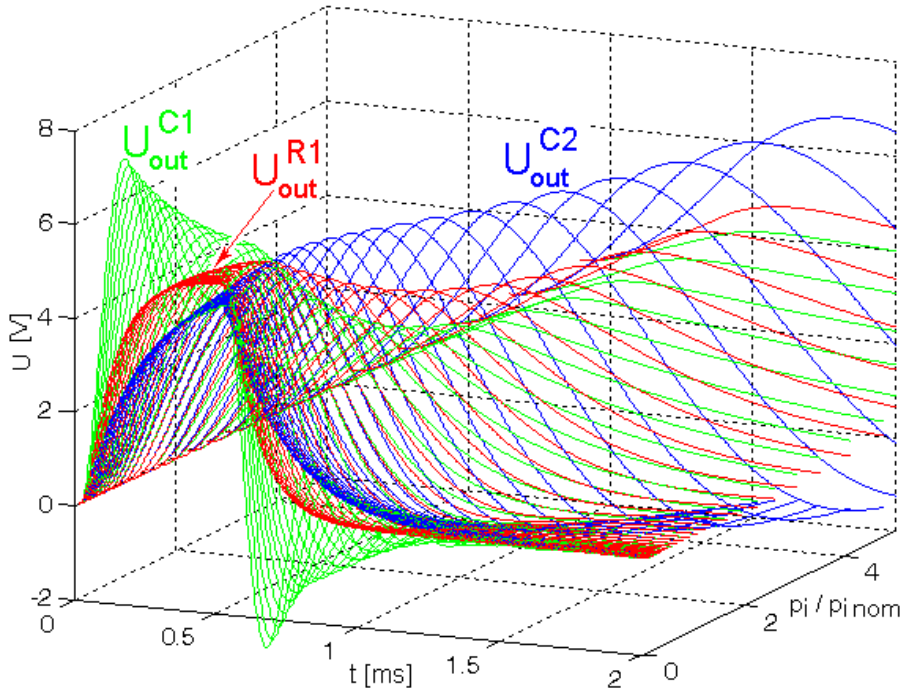

Fig. 2. Sets of time responses of the Sallen-Key low pass filter (Fig. 1) for changes of values of R_1, C_1 and C_2 elements from 0.1 to 5 of their nominal values

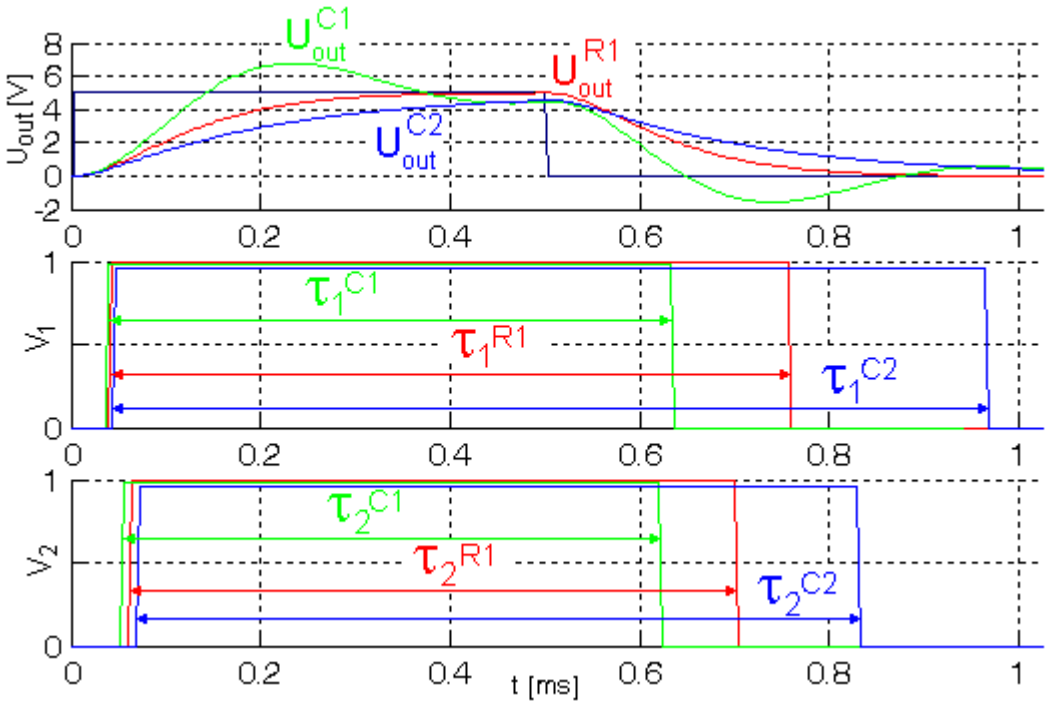

Fig. 3. Time responses of the analog circuit for 0.2 nominal values of R_1, C_1 and C_2 elements, and digital signals V_1 and V_2 at the outputs of the respective analog comparators

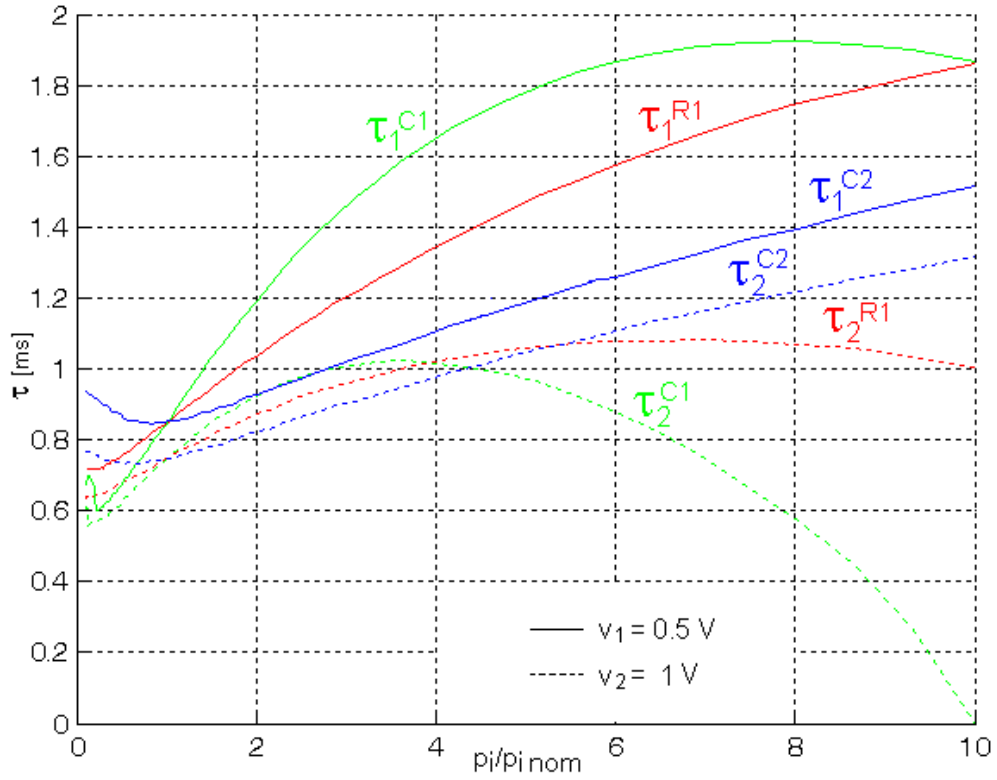

Fig. 4. Charts of duration times τ_k^i in function of all elements' values and threshold voltages v_1 and v_2

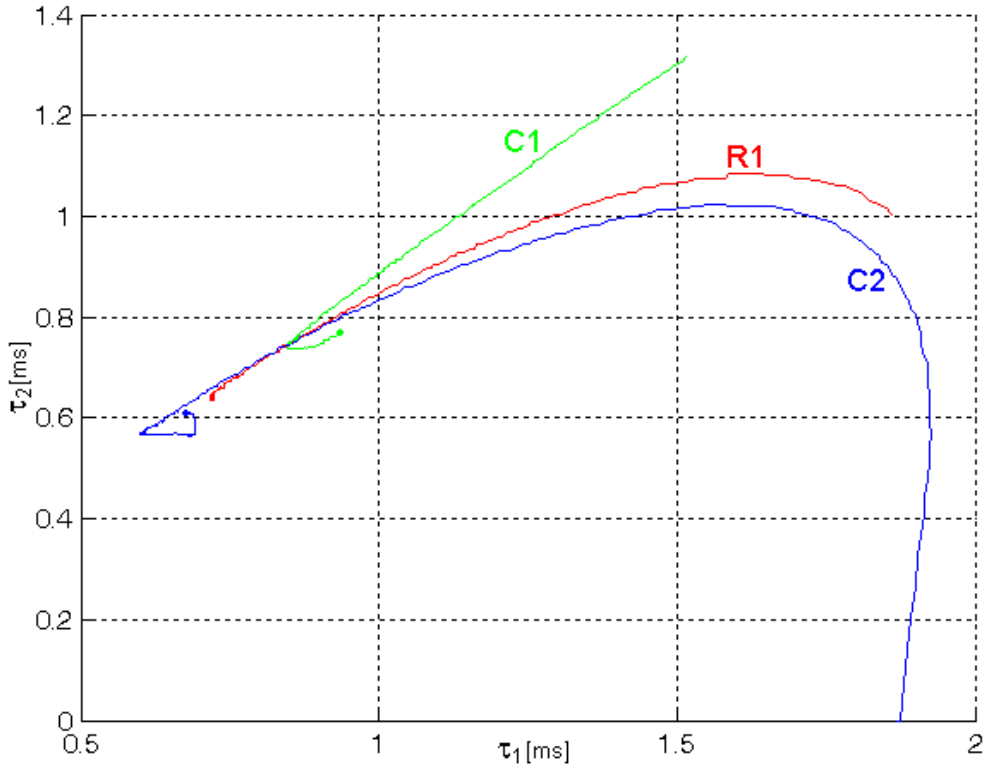

Fig. 5. Map of localization curves for the circuit (Fig. 1) in the 2-dimensional measurement space (K=2)

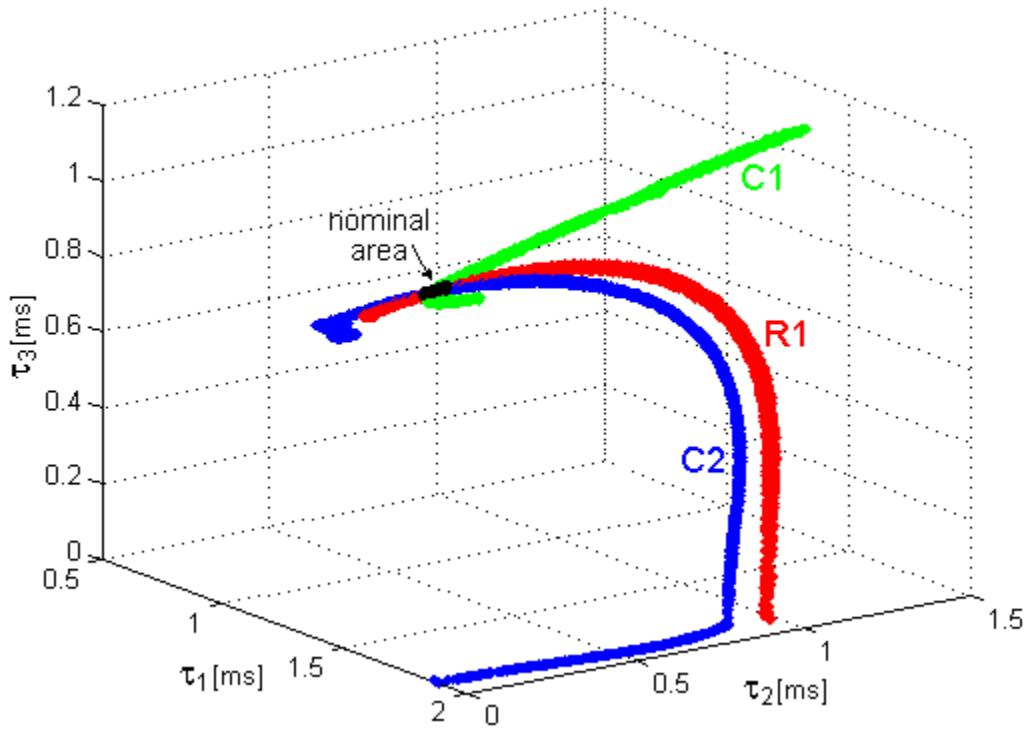

Fig. 6. Map of localization snakes for the circuit (Fig. 1) in the 3-dimensional measurement space (K=3) for 1% tolerances of resistors and 5% tolerances of capacitors

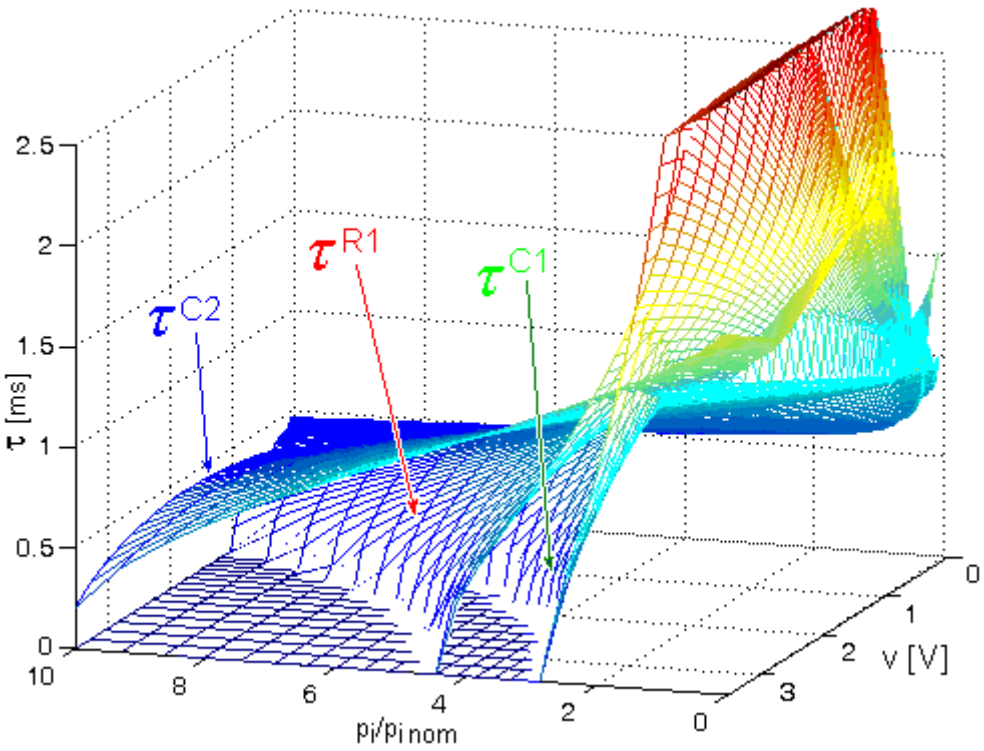

Fig. 7. Charts of duration times τ^i as a function of changes of elements' values $p_i/p_{i\,nom}$ and values of the threshold voltage v

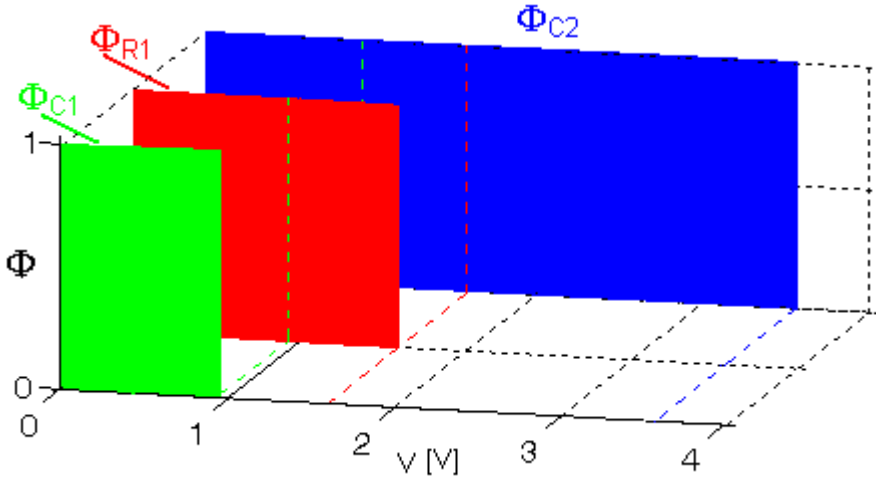

Fig. 8. Charts of Φ_i coefficients for R_1, C_1 and C_2 elements as a function of the threshold voltage v

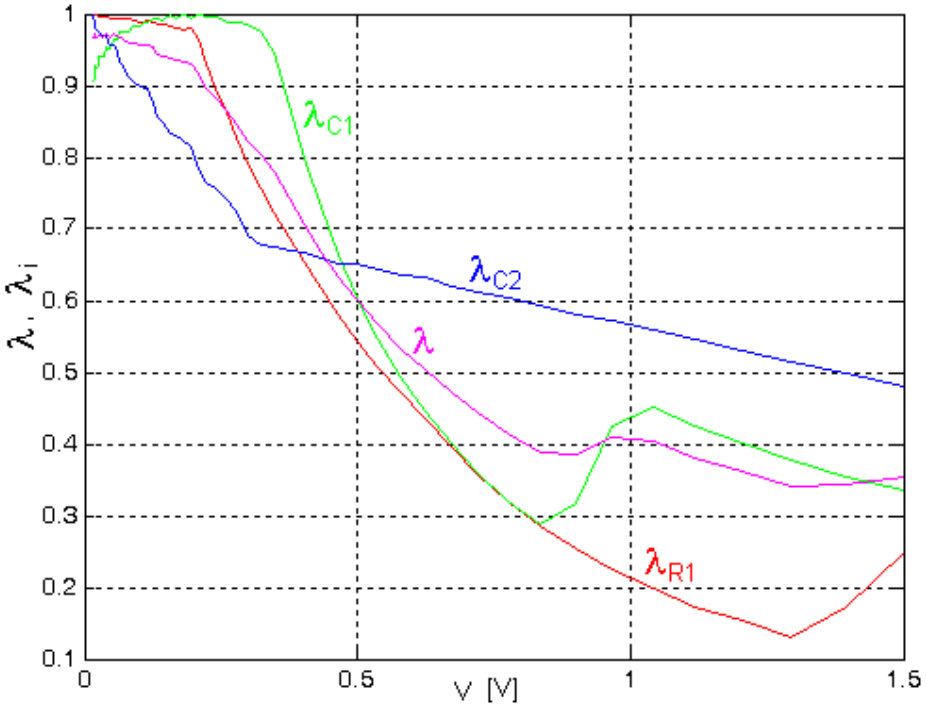

Fig. 9. Charts of the λ coefficient and λ_i coefficients for R_1, C_1 and C_2 elements as a function of the threshold voltage *v*

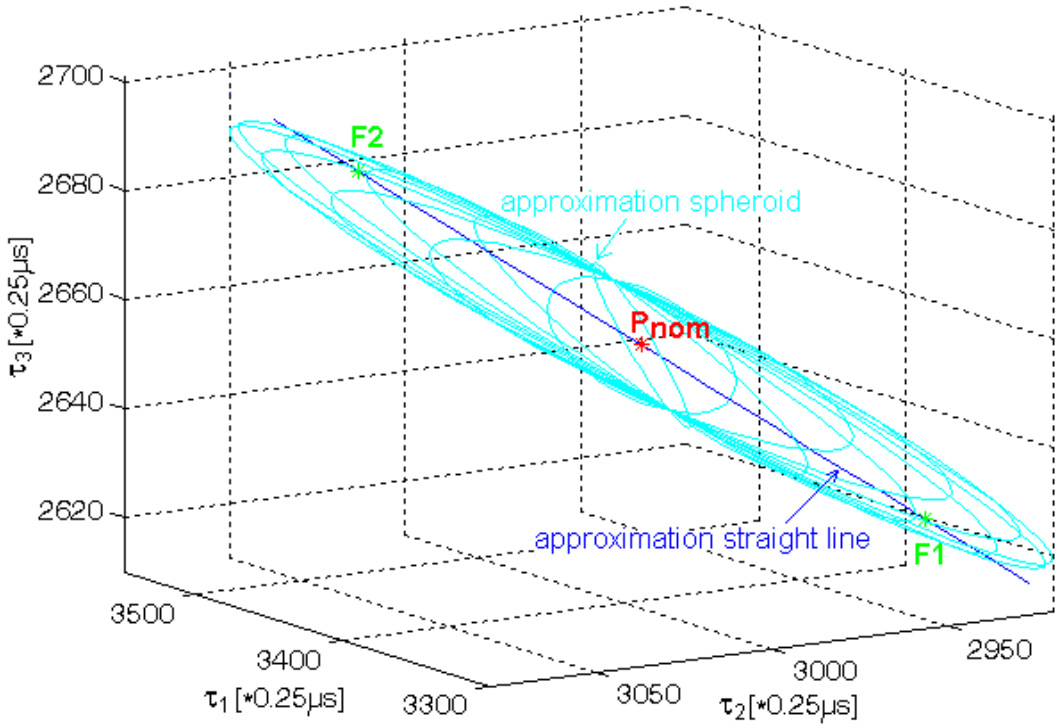

Fig. 10. The approximation spheroid of the nominal area in the measurement space

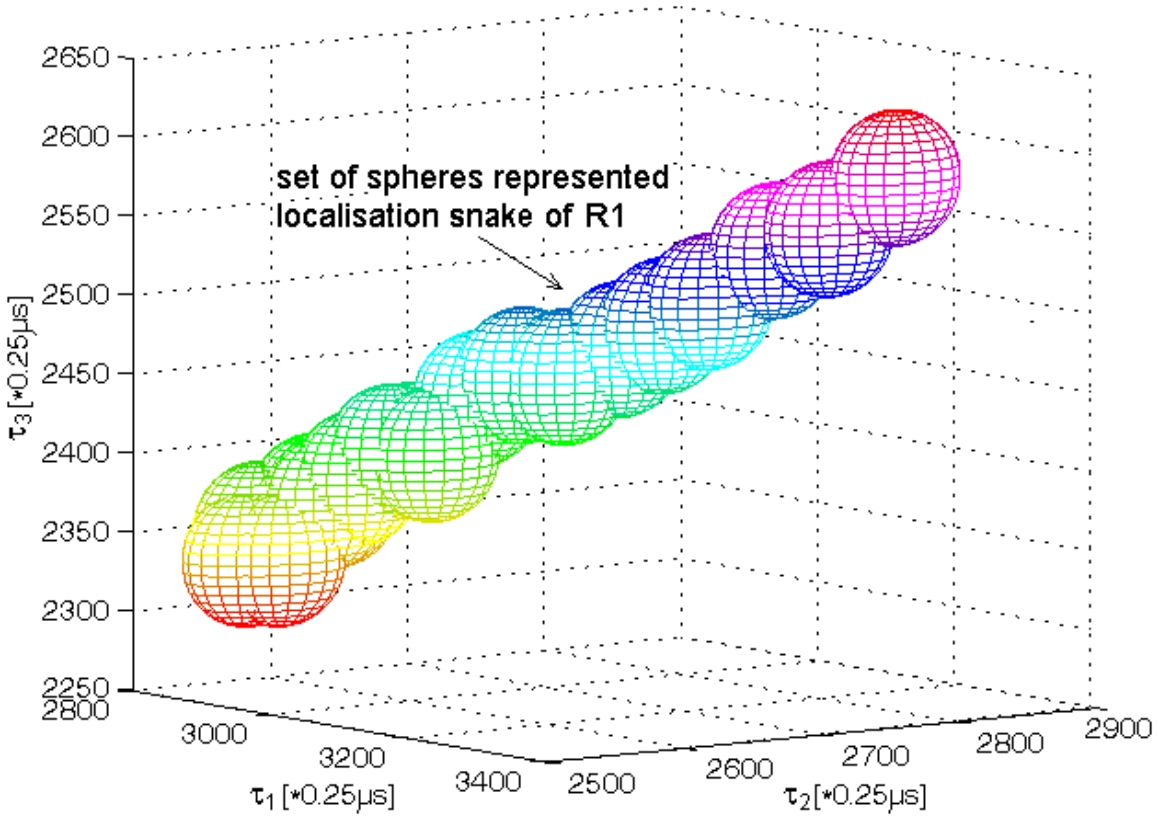

Fig. 11. The way of approximation of the localization snake by the set of spheres

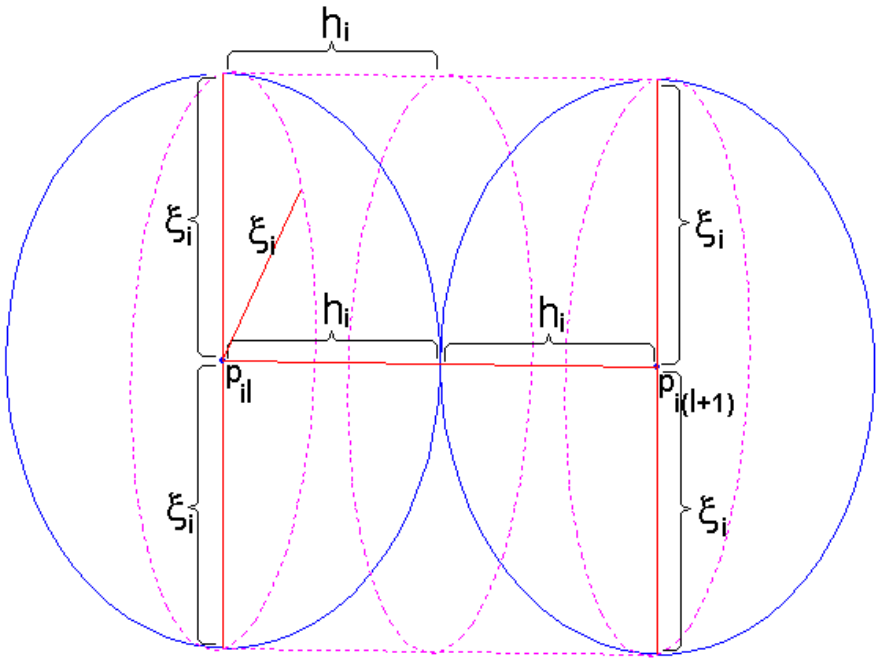

Fig. 12.The approximation spheres with radius ξ_i and the centre p_{il} and $p_{i(l+1)}$ contained in the cylinder with radius ξ_i and height $2h_i$ where $h_i \leq \xi_i$

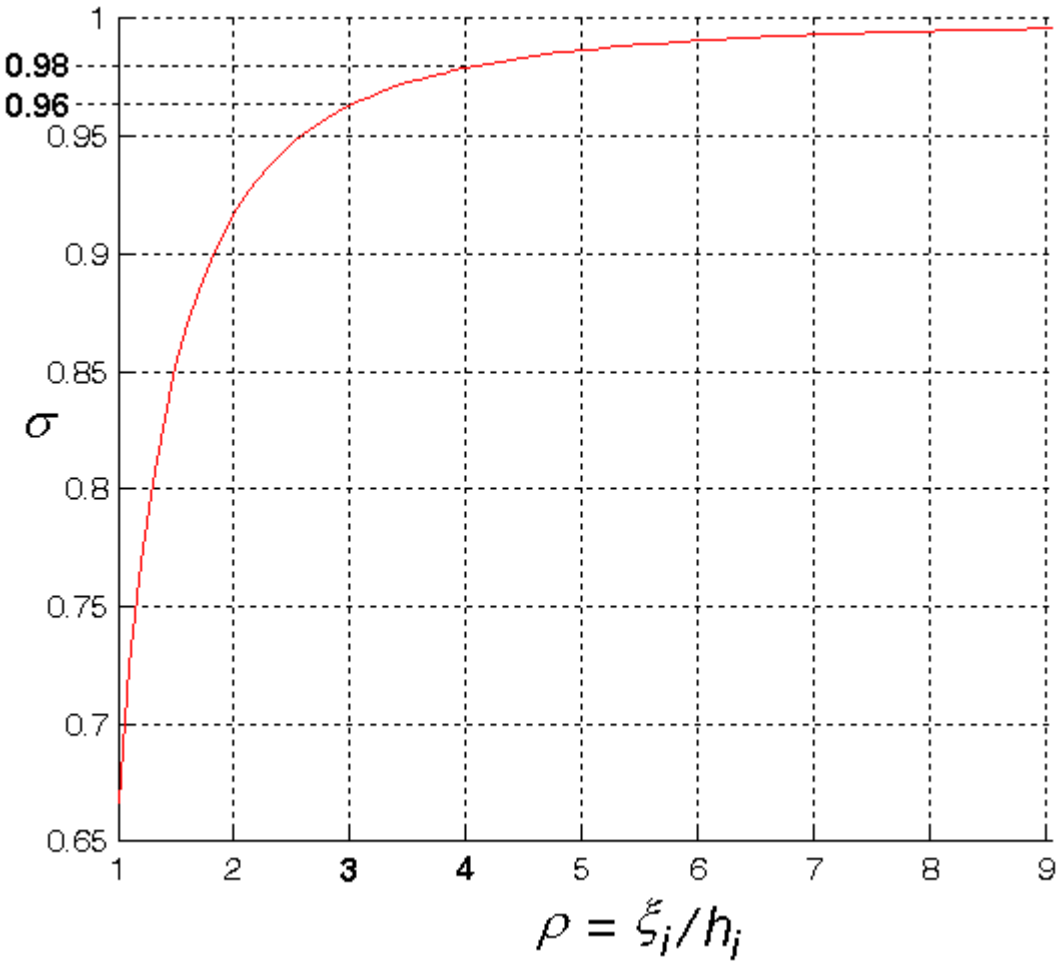

Fig. 13. Graph of the coefficient σ of fault localization closeness in function of the coefficient $\rho = \xi_i / h_i$ represented additional concentration of approximation spheres

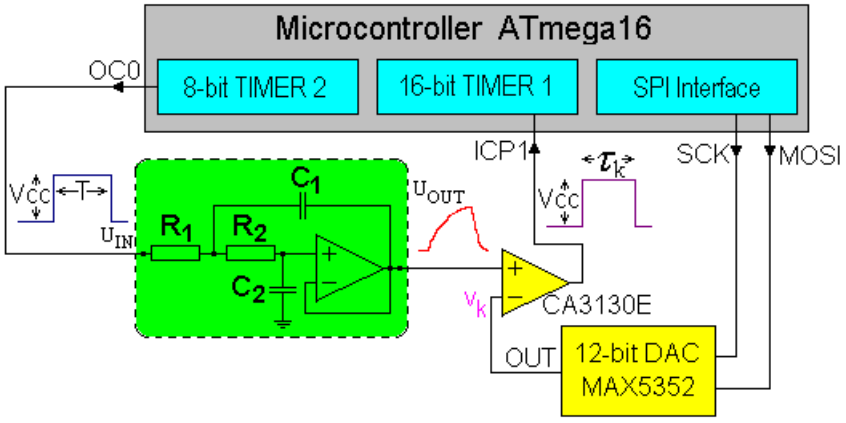

Fig. 14. Laboratory system with the tested analog part

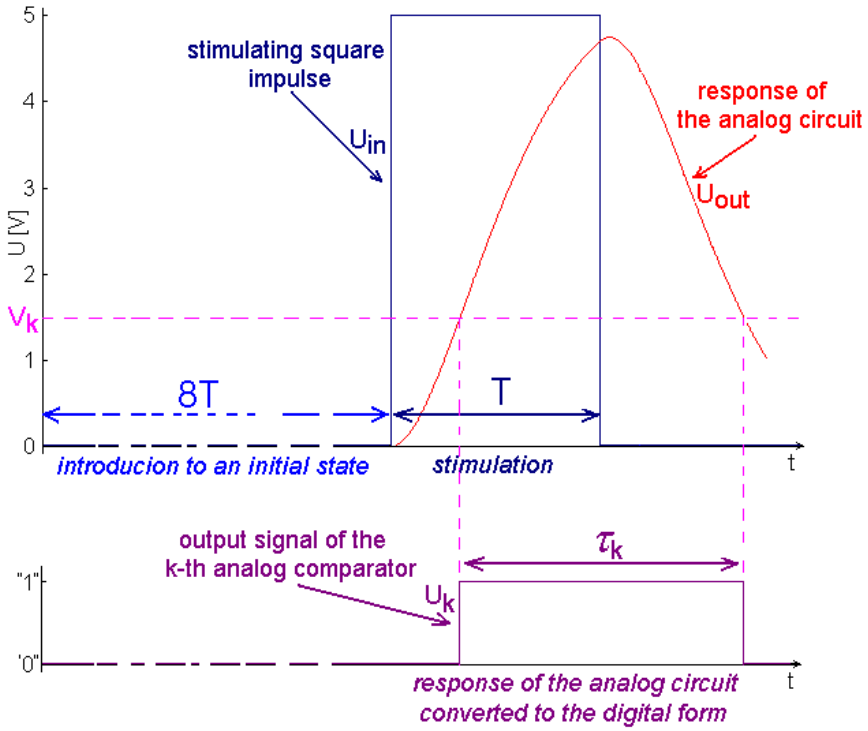

Fig. 15. Timings of the U_{in}, U_{out} and V_k during execution the measurement function by the microcontroller

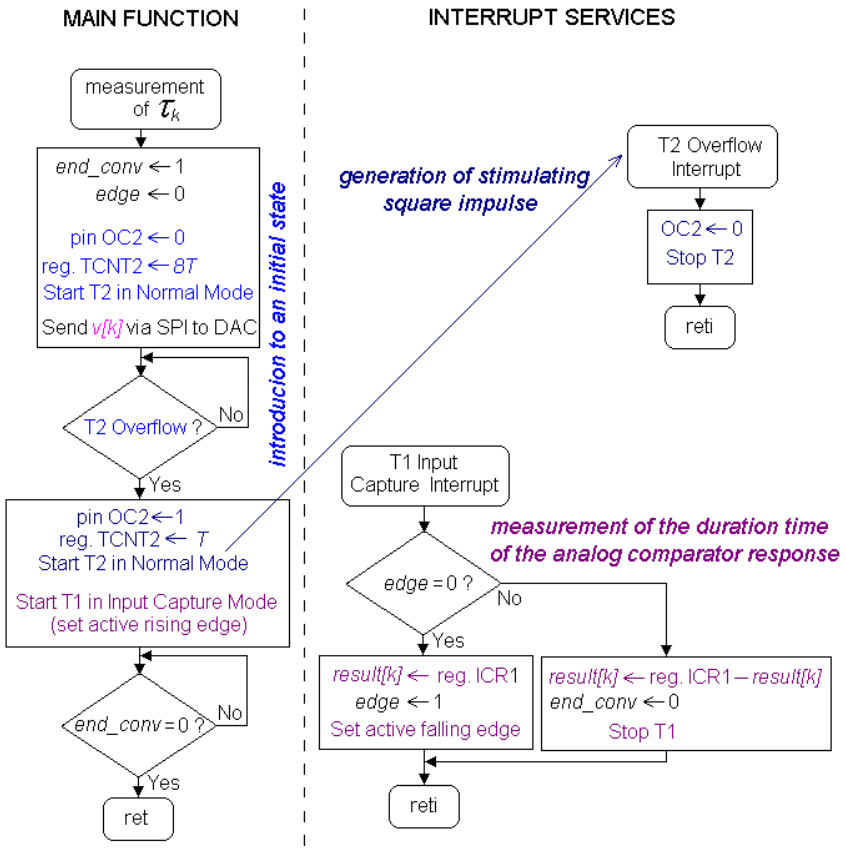

Fig. 16. The algorithm of the measurement function

Nr. of bit	8	7	6	5	4	3	2	1
Fault	*nom*	-	-	-	*C2*	*C1*	*R2*	*R1*

Fig. 17. A way of coding of respective faults in the byte variable *fdresult*

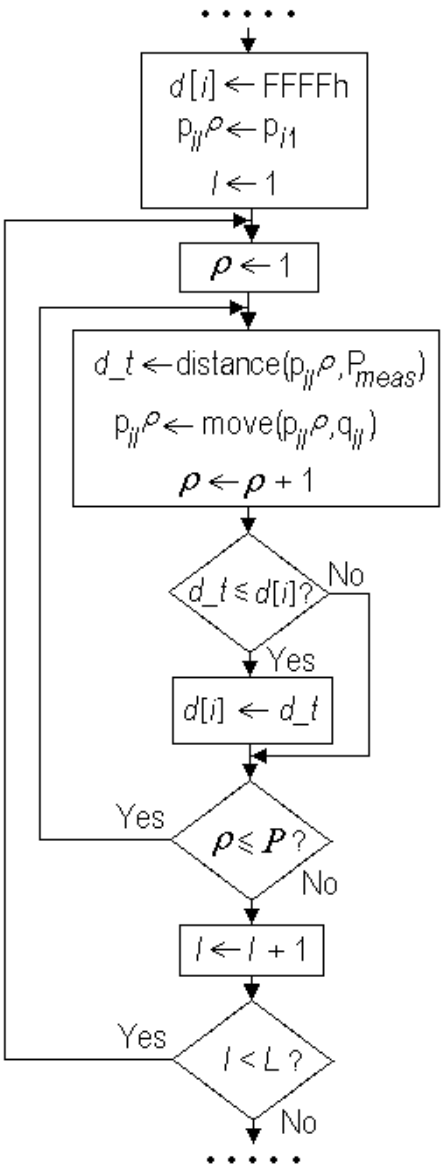

Fig. 18. A fragment of the fault localization algorithm showing a way of determination of the distance d_i between the measurement point P_{meas} and the i-th localization curve

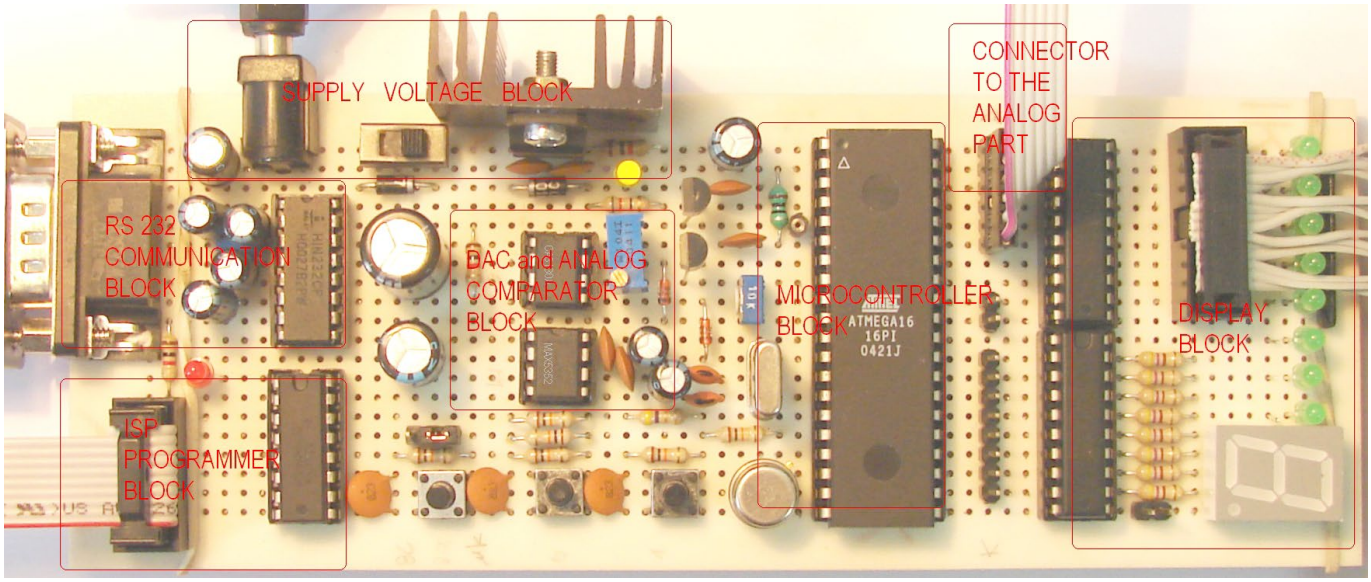

Fig. 19. A picture of the laboratory embedded electronic system based on the ATmega16 microcontroller

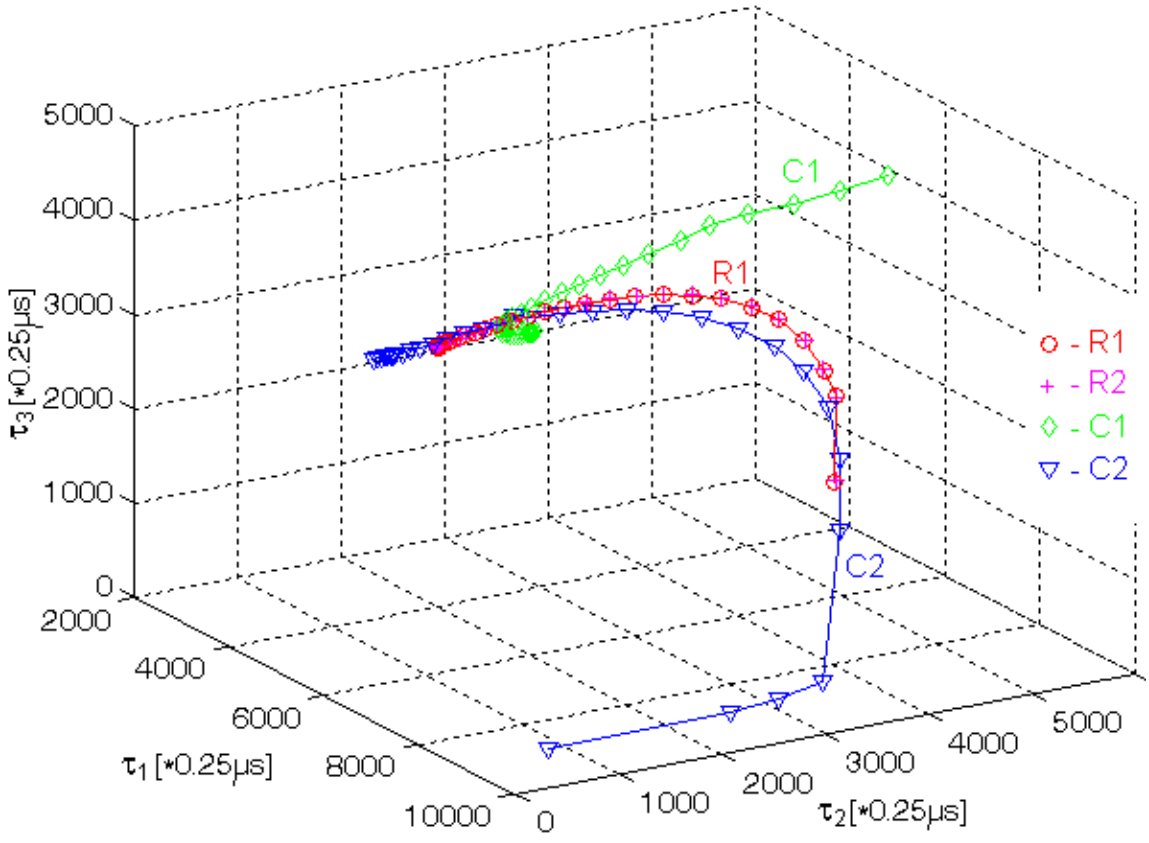

Fig. 20. Map of experimental localization curves for the circuit (Fig. 14) together with measurement points in the measurement space